Catchments as simple dynamical systems: Experience from a Swiss prealpine catchment

A. J. Teuling,[1,2] I. Lehner,[1] J. W. Kirchner,[3,4] and S. I. Seneviratne[1]

Received 3 November 2009; revised 7 June 2010; accepted 17 June 2010; published 6 October 2010.

[1] Heterogeneity in small-scale subsurface flow processes does not necessarily lead to complex system behavior at larger scales. Here we use the simple dynamical systems approach recently proposed by Kirchner (WRR, 2009) to analyze, characterize, and simulate streamflow dynamics in the Swiss Rietholzbach catchment. The Rietholzbach data set used here provides 32 years of continuous and high-quality observations, which include a soil moisture profile and unique observations of storage changes and evapotranspiration measured by a weighing lysimeter. Streamflow recession at the daily time scale shows a marked seasonal cycle and is fastest in summer due to the higher evapotranspiration losses. The discharge sensitivity function linking storage and discharge is nonlinear and slightly downward-curving in double-logarithmic space. Small diurnal discharge fluctuations prevent application of the approach at the hourly resolution for low-discharge conditions. The vast majority of runoff peaks can be explained by storage variations, except peaks that follow events with extreme precipitation intensity (30–40 mm h^{-1}). Storage change dynamics inferred from streamflow variations compare well to observations from the lysimeter and simulations with a land surface model but become very uncertain under dry conditions. Good results can be obtained when the discharge sensitivity function is calibrated on a monthly time scale to avoid the effect of the diurnal discharge fluctuations. Our analysis highlights the importance of evapotranspiration for catchment hydrology, as it is the main driver of changes in streamflow at Rietholzbach for 21% of the time.

Citation: Teuling, A. J., I. Lehner, J. W. Kirchner, and S. I. Seneviratne (2010), Catchments as simple dynamical systems: Experience from a Swiss prealpine catchment, *Water Resour. Res.*, *46*, W10502, doi:10.1029/2009WR008777.

1. Introduction

[2] Catchments are the key landscape elements for the analysis of water fluxes. This is not least because the convergence of flow into a stream allows for easy monitoring of water fluxes at the catchment outlet. Catchments are also the natural filters that control how variability in atmospheric conditions is translated into variations in streamflow. Governing flow equations, such as the Darcy equation or Richards' equation, have all been derived at scales several orders of magnitude smaller than the catchment scale and without taking into account variability in natural porous media or nonmatrix flow. The modeling of catchment processes is complicated due to several factors. Not only are model parameters spatially heterogeneous and hard to measure; also the optimal model structure may change with the scale at which models are applied [*Kirchner*, 2006].

[3] Traditionally, hydrological models have been developed around the central assumption that the functional behavior of hydrological systems can be predicted solely from physical properties of the system, combined with the governing flow equations and initial and boundary conditions. Over the past decades, the limitations of this approach have become clear. System properties cannot be easily determined a priori at the appropriate scale, and model parameters need to be optimized in order to achieve a satisfactory correspondence between observed and simulated fluxes. Observed fluxes are however not yet routinely used to infer information concerning model structure. It has been suggested that a downward approach, where time series characteristics are used to derive model structures rather than to optimize parameters of a given model structure, should play a more prominent role in model development and process identification [*Sivapalan et al.*, 2003].

[4] In a recent study, *Kirchner* [2009] proposed to represent catchments as simple dynamical systems, for which the model structure (i.e., the conceptualization of the system properties) can be directly inferred from observed changes in streamflow during recession. Here, simple refers to the fact that the combined effect of all subsurface flow processes on the catchment streamflow can be represented as resulting from a single state variable. The only (but necessary) assumption is that runoff is solely dependent on the total water storage in the catchment. This approach yielded

[1]Institute for Atmospheric and Climate Science, ETH Zurich, Zurich, Switzerland.
[2]Hydrology and Quantitative Water Management Group, Wageningen University, Wageningen, Netherlands.
[3]Swiss Federal Institute for Forest, Snow, and Landscape Research WSL, Birmensdorf, Switzerland.
[4]Institute of Terrestrial Ecosystems, ETH Zurich, Zurich, Switzerland.

0043-1397/10/2009WR008777

Table 1. Climate Summary for Rietholzbach

Variable	Mean Value
2 m air temperature[a]	7.1°C
Precipitation[a]	1459 mm yr^{-1}
Discharge[a]	1063 mm yr^{-1}
Evapotranspiration[a,b]	560 mm yr^{-1}
Evapotranspiration[c]	396 mm yr^{-1}
Potential evapotranspiration[d]	501 mm yr^{-1}
Relative humidity	80.2%
Wind speed[a]	1.36 m s^{-1}

[a]Taken from S. I. Seneviratne et al. (manuscript in preparation, 2010).
[b]Value for lysimeter.
[c]Value based on the long-term difference between precipitation and discharge.
[d]Calculated by the Priestley-Taylor equation.

good results for two catchments at Plynlimon in Mid Wales [*Kirchner*, 2009]. Moreover, the simplicity of the system allowed for "doing hydrology backward," i.e., estimation of fluxes at the land surface from variations in streamflow. Recession analysis has been widely used to study properties of groundwater systems [*Hall*, 1968; *Tallaksen*, 1995; *Lyon et al.*, 2009], and recently also evapotranspiration recession has been used to study unsaturated zone properties [*Teuling et al.*, 2006]. However it has been known for decades that the recession rate also depends on evapotranspiration fluxes.

[5] The link between the rate of evapotranspiration at the land surface and the rate of streamflow recession, through the amount of water stored in the subsurface, was already acknowledged in the 1970s by *Federer* [1973] and *Daniel* [1976]. This link was further explored by *Wittenberg and Sivapalan* [1999] for a catchment in southwest Western Australia, where the recession rate showed a marked seasonal cycle that could be attributed to evapotranspiration. It was however not until the study of *Kirchner* [2009] that these processes were explicitly linked in a simple framework without the need for calibration or baseflow separation. The method presented by *Kirchner* [2009] offers some interesting possibilities for new approaches to catchment hydrology that were not explored in depth before, but it relies on the assumption of hydraulic connectivity between the main dynamical saturated and unsaturated stores in the catchment. Whether this assumption is justified can be tested by applying the method to catchments with different climate and subsurface conditions.

[6] Here, we test whether the Swiss Rietholzbach catchment (S. I. Seneviratne et al., manuscript in preparation, 2010) behaves like a first-order dynamical system. Like the Plynlimon catchments, Rietholzbach can be classified as humid. However, the Rietholzbach catchment receives considerably less precipitation than Plynlimon does, and the observational record at Rietholzbach contains some severe droughts (e.g., 1976, 1991, 2003). In the presentation that follows, we first focus on the discharge sensitivity function, which describes the sensitivity of discharge to changes in catchment storage. This function fully characterizes the first-order system. Next, we infer catchment storage from streamflow, and compared it to other estimates including unique observations from a weighing lysimeter. Discharge is also simulated. Finally, the discharge sensitivity function is used to infer infiltration (precipitation and snowmelt) rates from fluctuations in streamflow.

2. Catchment Description and Data

[7] Observations in this study come from the Rietholzbach catchment in northeastern Switzerland (47.37°N, 8.99°E). For more information on the catchment and observations we refer to S. I. Seneviratne et al. (manuscript in preparation, 2010), *Lehner et al.* [2010], and www.iac.ethz.ch/url/rietholzbach. The small hilly prealpine basin (altitude range 682–950 m) has a drainage area of 3.31 km^2 and receives an average annual precipitation of 1459 mm. (Partial) snow cover is common in winter. A summary of basic climate characteristics is provided in Table 1.

[8] The parent rock types (mainly limestone and dolomite conglomerates) and the pronounced relief have produced a large variety of soil types. They can be summarized in a group of gley soils (42% of the area, mainly in the lower catchment parts) and a group of regosols and cambisols (58% of the area, mainly on the slopes). Soil depth is highly variable and ranges from less than 0.5 m on the steep slopes up to more than 2 m in the valley bottom [*Germann*, 1981]. Land use in the Rietholzbach catchment underwent no major changes since the start of the observations. The basin is mainly used as pasture (73%); about one fourth is (coniferous) forest. Population in the area is sparse. Humid conditions prevail throughout the year, resulting in a high correlation between evapotranspiration and the available radiative energy [*Teuling et al.*, 2009].

[9] Observations in the catchment started in 1975, and include runoff, radiation, soil moisture, standard meteorological variables, stable water isotopes, and groundwater. Here we use observations at the hourly resolution for the period 1976–2007. The hourly resolution is larger than the typical travel times of the stream, yet much smaller than the typical response time scale of the system even under extremely wet conditions (see section 5). A weighing lysimeter (diameter 2 m, depth 2.5 m) installed in the catchment measures weight (storage) with an equivalent accuracy of 0.1 mm of water. The lysimeter data have previously been used for model validation [*Calanca*, 2004], to detect long-term impacts of changes in radiation on evapotranspiration [*Teuling et al.*, 2009], and to analyze water balance closure of the catchment [*Lehner et al.*, 2010]. The main gauge "Rietholzbach-Mosnang" at the outlet of the basin is operated by the Federal Office for the Environment (Hydrology Division, Bern, Switzerland).

[10] Simulations were performed with the Variable Infiltration Capacity model [version *Liang et al.*, 1994]. Forcing was either taken from the observations, or from the 15 year atmospheric reanalysis provided by the ECMWF (ERA-15). Default parameters were used based on the predominant soil type in the region (FAO classification) and no calibration was performed.

3. System Characterization by Discharge Sensitivity

[11] We start off by assuming that the water balance for the total liquid subsurface storage (both saturated and

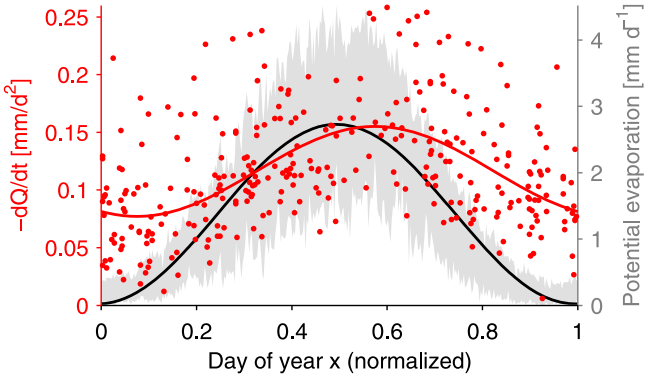

Figure 1. Impact of evapotranspiration on the streamflow recession for Rietholzbach. Points indicate the recession $-dQ/dt$ estimated from change in daily average discharge over any two subsequent days in the period 1976–2007 without rainfall and for which the average discharge was around 1 mm d^{-1}. The shaded area indicates the daily potential evapotranspiration for the same period (mean ± standard deviation). The curves are fitted sine functions. See text for details.

unsaturated) in the catchment is adequately represented by:

$$\frac{dS}{dt} = I - ET - Q = P + M - ET - Q, \tag{1}$$

where I is the surface infiltration consisting of infiltration due to liquid precipitation (P) and snowmelt (M), ET is the total evapotranspiration (soil evaporation and transpiration), and Q is the discharge at the catchment outlet. Flow across the borders of the catchment, except via streamflow, is neglected. This is a reasonable assumption given the steep slopes and shallow soils near the topographic watershed boundary. We assume interception of precipitation by vegetation to be negligible.

[12] In the analysis that follows, we will make one key assumption regarding the catchment behavior. Following *Kirchner* [2009], it is assumed that there is some unique (i.e., no hysteresis), but unknown, function $f(S)$ that relates the discharge at the catchment outlet Q to the total subsurface storage in the catchment S, i.e., $Q = f(S)$ or $S = f^{-1}(Q)$. Note that this assumption does not imply that catchment properties and fluxes are spatially homogeneous, or that small-scale processes such as pipeflow are unimportant in controlling the hydrological response of smaller areas within the catchment. It merely implies that small-scale processes can be scaled up to a unique relationship at the catchment scale, or that the occurrence of processes such as pipeflow depends on storage and can as such be implicitly parameterized at the catchment scale. It also implicitly implies that a hydraulic connection exists between the saturated and unsaturated storage in the catchment. Such a connection has been confirmed both by experimental and theoretical studies [*Beldring et al.*, 1999; *Bogaart et al.*, 2008].

[13] An obvious problem with $f(S)$ is that the total subsurface storage S cannot be estimated accurately at the appropriate (catchment) scale. Also, subsurface storage is an ill-defined quantity due to the lack of a clear lower system boundary. An alternative to using direct observations of storage was presented by *Kirchner* [2009] and uses the derivative of $f(S)$ rather than $f(S)$ directly:

$$f'(S) = \frac{dQ}{dS} = f'\left(f^{-1}(Q)\right) = g(Q). \tag{2}$$

The function $g(Q)$ will be called the "discharge sensitivity" hereafter. It is equivalent to the "sensitivity function" in the work of *Kirchner* [2009]. It expresses the sensitivity of discharge to changes in storage as function of discharge (which is observable) rather than storage (which is not). Using the above-derived $g(Q)$ and substituting dS/dt with the water balance equation (1), we obtain the following differential equation for changes in discharge [*Kirchner*, 2009]:

$$\frac{dQ}{dt} = \frac{dQ}{dS}\frac{dS}{dt} = g(Q) \cdot (P + M - ET - Q). \tag{3}$$

Thus, equation (3) relates the discharge sensitivity to fluxes only. In section 5, we will focus on the question how this function can be estimated from observations.

4. Relation Between System Losses and Recession

[14] A first qualitative confirmation that the Rietholzbach indeed behaves like a first-order dynamical system can be obtained by looking at the rate of streamflow recession. Without any prior knowledge on the shape of $g(Q)$, equation (3) already predicts that at a given storage level, the recession rate $-dQ/dt$ depends on the system state S (or equivalently Q) and ET:

$$-\frac{dQ}{dt} = g(Q) \cdot (ET + Q). \tag{4}$$

While the catchment behavior cannot be analyzed at a given storage level, it is possible to analyze the recession behavior within a narrow range of Q, so that $g(Q)$ is approximately constant. Figure 1 shows the rate of recession $-dQ/dt$ for daily average discharge (i.e., with the diurnal cycle impact of ET removed) calculated for any two subsequent dry days for which the average discharge is within a narrow range (centered around 1 mm d^{-1} ± 0.1 on the natural log scale). Note that recession time scales depend on discharge, so binning the recession time scales into narrow bins of Q is necessary to remove the impact of Q. The seasonal cycle of potential evaporation as a proxy for actual ET is plotted for reference. To both variables, we fitted the following sine function:

$$f(x) = c_1 + c_2 \sin(2\pi(x - c_3)), \tag{5}$$

where x is the normalized day of year and c_i are fitting parameters. For the recession rate, robust fitting resulted in the following parameters: $c_1 = 0.12 \pm 0.01$, $c_2 = 0.04 \pm 0.01$, and $c_3 = -0.32 \pm 0.03$. For potential evaporation, the parameters obtained with least squares fitting were $c_1 = 1.38 \pm 0.02$, $c_2 = 1.35 \pm 0.02$, and $c_3 = -0.24 \pm 0.00$.

[15] The rate of streamflow recession shows a clear seasonal dependency, with slower streamflow recession in the cold season (due to small additional evapotranspiration losses) and faster recession in the warm season (due to larger evapotranspiration losses). For the selected range in Q, evapotranspiration exceeds streamflow in summer by a

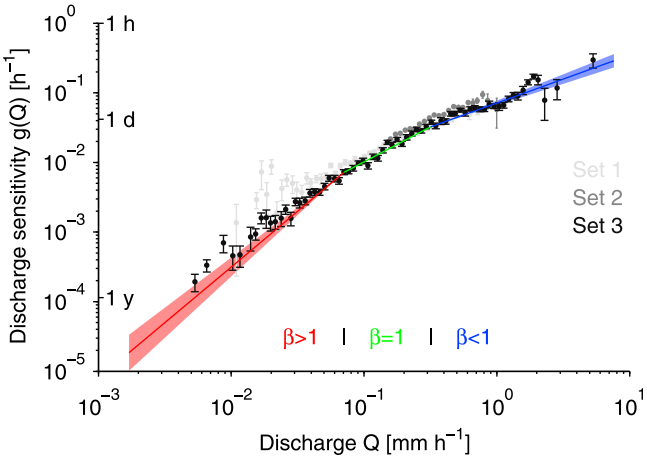

Figure 2. Observed discharge sensitivity $g(Q)$ for Rietholzbach. Points and error bars indicate bin averages and standard errors, respectively, for the three subsets of data (see text for details). The piecewise linear fit reflects power law behavior over parts of the domain. For the middle section $\beta = 1$ (see equation (9)).

factor of two (2–3 mm d^{-1}). For this situation, equation (4) predicts that in summer, with losses by both Q and ET, the recession $-\mathrm{d}Q/\mathrm{d}t$ should be roughly three times as rapid as during winter. This is consistent with the results of the regression, where a three times larger $-\mathrm{d}Q/\mathrm{d}t$ falls within the uncertainty of the parameters. Furthermore the minima in the regression are nearly in phase. While the qualitative effect of increasing evapotranspiration on streamflow recession curves is well documented [e.g., *Federer*, 1973; *Wittenberg and Sivapalan*, 1999], it is important to note that also quantitatively this effect is consistent with the impact of evapotranspiration on storage depletion. These results give a first indication of the importance of evapotranspiration and storage in regulating streamflow in the Rietholzbach catchment. Next, we will explore and quantify this link further.

5. Discharge Sensitivity From Observations

[16] In our system characterization, the discharge sensitivity completely determines the catchment behavior. In contrast to "traditional" hydrological models, however, its behavior is not based on observed physical properties of the system or calibrated parameters, but rather on observed fluxes. While this may seem overly simple, it should be noted that by definition in this type of system all small-scale processes are implicitly accounted for by the discharge sensitivity. The discharge sensitivity can be estimated from observations as follows. Theoretically, $g(Q)$ can be estimated from equation (3) by monitoring all fluxes. Conceptually, this is done by isolating the catchment from all factors that cannot be measured. In practice, this isolation is done in the temporal domain by selecting time periods during which all fluxes to and/or from the catchment can be measured with sufficient accuracy or can be neglected. Since snowmelt and evapotranspiration are difficult to measure at the catchment scale, it is convenient to estimate $g(Q)$ at times when both fluxes can be neglected. During recession ($P = 0$ and $M = 0$), this yields:

$$g(Q) = \frac{\mathrm{d}Q}{\mathrm{d}S} \approx \left.\frac{-\frac{\mathrm{d}Q}{\mathrm{d}t}}{Q}\right|_{P,M,ET \ll Q}. \quad (6)$$

Alternatively, during rainfall, $g(Q)$ can be estimated through:

$$g(Q) = \frac{\mathrm{d}Q}{\mathrm{d}S} \approx \left.\frac{-\frac{\mathrm{d}Q}{\mathrm{d}t}}{P - Q}\right|_{M,ET \ll Q}. \quad (7)$$

[17] The selection of periods when evapotranspiration and snowmelt can be neglected requires attention. If the selection criteria are chosen too stringent, little data is left to estimate $g(Q)$ even with 32 years of hourly observations. On the other hand, too loose criteria might increase the contribution of snowmelt and evapotranspiration, and consequently lead to an overestimation and underestimation, respectively, of $g(Q)$. The lack of continuous snow observations at Rietholzbach is another complicating factor. To avoid any influence of snowmelt on $g(Q)$, the selection of data for the $g(Q)$ function was based on the following three sets of criteria:

[18] Set 1 is cold, dry, and dark. Moving-average temperature (4 h) is low enough (<0°C) to exclude snowmelt but high enough to exclude ice at the weir (>−3°C), and both 4 h moving average precipitation and global radiation are negligible.

[19] Set 2 is warm, dry, and dark. Moving-average temperature (previous 7 days) is high enough to exclude the presence of snow (>3°C), and both precipitation and evapotranspiration can assumed to be negligible. Days during which runoff is smaller than a given evapotranspiration threshold (0.15 mm h^{-1}) and during which evapotranspiration can have a significant impact on the nighttime recession (see section 12) are excluded.

[20] Set 3 is warm and raining. Average temperatures (previous 7 days) are high enough (>3°C) to exclude presence of snow, and precipitation rates are at least an order of magnitude larger than estimated maximum evapotranspiration rates (0.15 mm h^{-1}).

[21] By applying the above criteria, only 8% of the data in the 32 year record can potentially be used to estimated $g(Q)$. While this leaves a significant number of data points for 32 years of hourly data (nearly 23,000), it might limit the applicability of the method to basins with short observational records. Due to measurement errors, limited measurement precision, inherent natural variability and/or a possible difference in our conceptualization of the catchment and the real behavior, there is also considerable scatter in the data for all three sets. This scatter includes zero values as well as negative values. These effects (the scatter as well as zero and negative values) prohibit the fit of a discharge sensitivity curve in log space. Therefore, we bin the data for further analysis. For each set, bins are taken equally spaced in log space, but the bin size is increased locally whenever the standard error is too large, or whenever a bin average is negative.

[22] Figure 2 shows the inferred discharge sensitivity for Rietholzbach. It is worth noting first that the discharge

sensitivity is in fact highly dependent on discharge itself. This is not only true for recession data points, but also for the points that have been derived from the rising limb of the hydrograph (i.e., set 3). This strong dependency invalidates alternative conceptual approaches to runoff modeling at Rietholzbach, such as a linear reservoir (where the discharge sensitivity would be a constant) or the unit hydrograph approach (which does not consider the catchment to be a dynamical system). Secondly, the bin averages for the three sets of data selection criteria largely overlap. Since the bin averages for one set (3) originate from the rising limb of the hydrograph and the others (1,2) from recession, there is no indication for a strong hysteresis in the relation between catchment storage and streamflow. Thirdly, on a double logarithmic scale there is a concave-downward tendency in the bin averages (here represented by a piecewise linear curve). A similar concave tendency was also reported by *Kirchner* [2009] for one of the Plynlimon catchments.

[23] We describe the dependency of the bin average streamflow sensitivity on streamflow by a piecewise linear fit in log-log space, i.e., by a piecewise power law in the linear space:

$$g(Q) = \alpha Q^{\beta}. \tag{8}$$

[24] Since there are some fundamental differences in system behavior for $\beta > 1$, $\beta = 1$ and $\beta < 1$ (see discussion in the work of *Kirchner* [2009]), we separate our representation of $g(Q)$ into these three ranges. Due to the concave tendency of $g(Q)$, we can conveniently define a central part of the curve for which $\beta = 1$. For the Rietholzbach, this part also corresponds to the range of Q where Q is most frequent (see inset in Figure 10), and where estimates of $g(Q)$ show least variability.

[25] By assuming that the uncertainty in the fit where $\beta \approx 1$ can be neglected when compared to the uncertainty in the wet and dry extremes where $\beta > 1$ and $\beta < 1$ (note that the dry and wet extremes have fewer observations than the range where $\beta \approx 1$), the error propagation is simplified considerably. In the following we will therefore only consider the error in the outer parts of $g(Q)$. While the piecewise power law has the drawback of having many degrees of freedom and discontinuities in its derivative, it allows for analytical expressions further on and avoids nonphysical behavior outside the fitting range.

[26] It should also be noted that α and β in $g(Q)$ are different from the parameters a and b in the "classical" recession analysis [*Brutsaert and Nieber*, 1977] where $-\mathrm{d}Q/dt$ rather than dQ/dS is plotted versus Q. The parameters b and β are related through $b = \beta + 1$.

[27] Based on equation (8) and the considerations above, we find the following relation for $g(Q)$ at Rietholzbach:

$$g(Q) = \begin{cases} 0.499Q^{1.6} & Q < 0.071 \\ 0.102Q & 0.071 \le Q < 0.317 \\ 0.071Q^{0.69} & Q \ge 0.317, \end{cases} \tag{9}$$

where $g(Q)$ is in h^{-1} and Q in mm h^{-1}. For the quadratic model used by *Kirchner* [2009], we find the following fit: $\ln(g(Q)) = -2.513 + 0.6421 \ln(Q) - 0.0796 (\ln(Q))^2$. Over the whole domain, the $g(Q)$ for the Plynlimon catchments is steeper than for Rietholzbach, and the $g(Q)$ is larger under wet conditions for Plynlimon ($Q > 1$ mm h^{-1}) because of the larger concavity in $g(Q)$ for Rietholzbach. This difference corresponds to a higher sensitivity of Q to changes in S for Plynlimon under wet conditions (at a given discharge level).

[28] In the case of nonconstant $g(Q)$, the apparent system response time or "memory" (in absence of forcing) depends on the system state (Q or S) and equals $g(Q)^{-1}$. Under near-saturated conditions, the system response time for Rietholzbach is on the order of only several hours. Under dry conditions, the response time rapidly increases to months or even years (see annotations in Figure 2). It should be noted that the actual time constant of streamflow recession will be smaller than $g(Q)^{-1}$ due to additional evapotranspiration losses (see also section 4).

6. Discharge Simulation

[29] When the discharge sensitivity is known, it is no longer necessary to implicitly account for the propagation of forcing through the storage reservoir in the simulation of streamflow. Streamflow can be simulated directly since $g(Q)$ explicitly accounts for the effects of the storage reservoir [see *Kirchner*, 2009]. In theory, equation (3) can be used directly to simulate Q. Due to the strong nonlinearity of $g(Q)$ however, simulating changes in $\ln(Q)$ rather than Q results in increased numerical stability [*Kirchner*, 2009]:

$$\frac{\mathrm{d}(\ln(Q))}{\mathrm{d}t} = \frac{1}{Q}\frac{\mathrm{d}Q}{\mathrm{d}t} = g(Q) \cdot \left(\frac{P + M - ET}{Q} - 1\right). \tag{10}$$

[30] Following *Kirchner* [2009], equation (10) is solved by using a fourth-order Runge-Kutta scheme with variable timesteps:

$$\ln(Q)_{n+1} = \ln(Q)_n + \frac{1}{6}h(s_1 + 2s_2 + 2s_3 + s_4), \tag{11}$$

where $h = t_{n+1} - t_n$ and $s_1, \ldots, s_4$ are subsequently calculated from:

$$s_1 = g[Q(t_n)] \cdot \left(\frac{P_n + M_n - ET_n}{Q(t_n)}\right), \tag{12}$$

$$s_2 = g\left[Q(t_n) + \frac{1}{2}hs_1\right] \cdot \left(\frac{P_n + M_n - ET_n}{Q(t_n) + \frac{1}{2}hs_1}\right), \tag{13}$$

$$s_3 = g\left[Q(t_n) + \frac{1}{2}hs_2\right] \cdot \left(\frac{P_n + M_n - ET_n}{Q(t_n) + \frac{1}{2}hs_2}\right), \tag{14}$$

$$s_4 = g[Q(t_n) + hs_3] \cdot \left(\frac{P_n + M_n - ET_n}{Q(t_n) + hs_3}\right). \tag{15}$$

[31] Note that P_n, M_n, and ET_n are discrete rather than continuous functions of time, and the numerical timestep required for stability will often be much smaller than the resolution of the input data. As a result, P_n, M_n, and ET_n will stay constant over several subsequent intervals $[t_n, t_{n+1}]$.

[32] In prealpine basins such as Rietholzbach, variations in temperature and radiation can have a large impact on

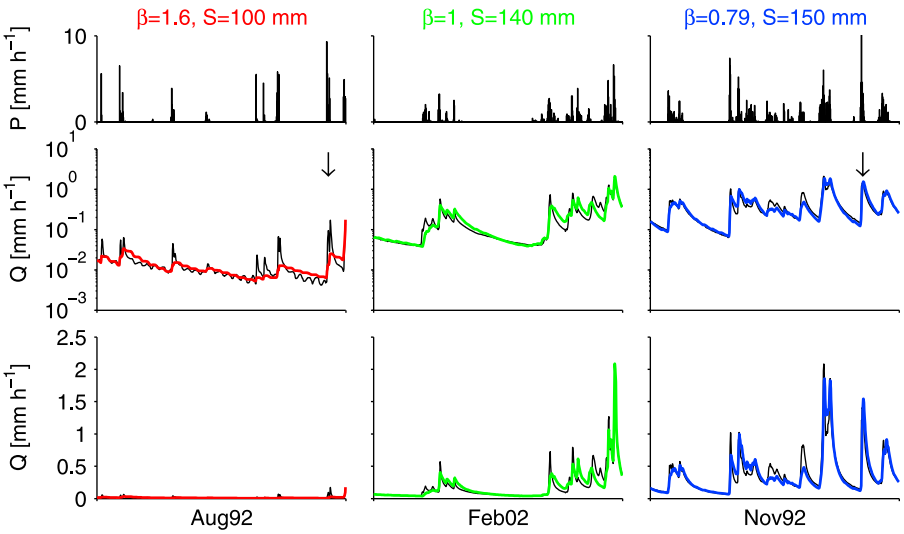

Figure 3. Observed and simulated discharge (Q) for Rietholzbach. (top) The observed hourly rainfall P. (middle and bottom) The observed (thin lines) and simulated (thick colored lines) hourly discharge in logarithmic and linear space, respectively. (left, middle, and right) The three cases illustrate the catchment response for months with characteristic storage regimes corresponding to different values of the power law exponent β (colors correspond to Figure 2). Values for S refer to monthly average storage inferred from equation (22). For each month, the parameters α, β, and ε were optimized, yielding $\alpha = -0.08$, $\beta = 1.64$, and $\varepsilon = 0.89$ (August 1992), $\alpha = -0.86$, $\beta = 1.01$, and $\varepsilon = -0.57$ (February 2002), and $\alpha = -1.11$, $\beta = 0.79$, and $\varepsilon = -0.88$ (November 1992). Note that ε can become negative in months where the potential evapotranspiration is negligible due to overcompensation.

streamflow through snowmelt [*Gurtz et al.*, 2003]. In the simulation of equation (10), infiltration is assumed to equal precipitation when the 2 m air temperature (T_{2m}) exceeds a reference temperature $T0$. When $T_{2m} < T0$, recorded rainfall is assumed to have fallen as snow, and the corresponding snow water equivalent is added to the snow water equivalent already present (if any). Snowmelt M is assumed to be driven by temperature and radiation only, and is parameterized by the restricted degree-day radiation balance approach [*Kustas et al.*, 1994]:

$$M = c_4(T_{2m} - T0) + c_5 R_g, \tag{16}$$

where R_g is the global radiation and c_i are fitting parameters. Note that in equation (16) we took global rather than net radiation since the latter is highly variable in catchments with variable and partial snowcover. We apply equation (16) at the hourly time scale in accordance with the resolution of the discharge observations.

[33] Catchment-scale evapotranspiration is estimated by the Priestley-Taylor equation:

$$ET = \varepsilon \cdot \alpha_e \frac{\Delta}{\Delta + \gamma}(R_n - G), \tag{17}$$

where ε is an evaporation efficiency, α_e the Priestley-Taylor constant (1.26), Δ the slope of the saturation water vapor pressure curve at T_{2m}, γ is the psychrometric constant (0.67 hPa K^{-1}), R_n is the net radiation and G is the ground heat flux. From available observations of ground heat flux, G was found to be a near-constant fraction (0.12) of R_n. In equation (17), the evaporation efficiency ε is a fitting parameter that includes both effects of phenology and soil moisture limitation on ET. From the long-term average water balance, we find $\varepsilon = 0.87$. Monthly values of ε are also obtained through optimization.

[34] Figure 3 shows the observed and simulated discharge for three selected months. These months have distinctively different storage regimes and relatively small variability, so that the assumption of a single power law function for $g(Q)$ is most appropriate (although discharge still varies over more than an order of magnitude). Figure 3 (left) shows a month with very low storage (August 1992), in which the optimized power law exponent is considerably larger than 1. Here, the discharge sensitivity is low, but changes rapidly with changes in storage. Comparison with observations reveals that the power law $g(Q)$ cannot capture the sharp peaks in streamflow in logspace. Due to the low sensitivity however, the response of Q to rainfall is extremely small for both simulations and observations in the linear space (Figure 3, bottom left).

[35] For higher levels of catchment storage, the catchment response to rainfall changes considerably, and the optimized power law exponent is near unity (as in February 2002, Figure 3, middle). Discharge now shows a distinct response to precipitation events that would have had hardly any effect on discharge under drier conditions. In this range, the fit between the simulated and observed discharge is good both in the linear and log space. In even wetter conditions (November 1992, Figure 3, right), the power law exponent decreases further so that the catchment sensitivity changes relatively little with changes in discharge. Note the good fit with the observed discharge in both log and linear space. Nash-Sutcliffe efficiencies for the log-transformed simulations (Figure 3, middle) are 0.60, 0.90, and 0.92, for August 1992, February 2002, and November 1992, respectively.

[36] Discharge simulations were also performed for the whole 32 year period based on equation (9). For this sim-

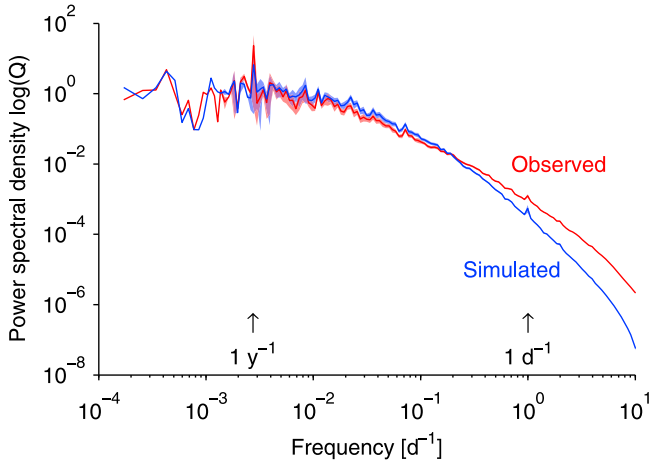

Figure 4. Spectral density of the natural logarithm of hourly observed (red) and simulated (blue) discharge. The discharge simulations were done using the observed (i.e., noncalibrated) discharge sensitivity (equation (9)). Note that the low-frequency (<10^0 d) response of the real system is well described by the system dynamical system model, but that differences occur at high frequencies.

ulation, snow parameters were first optimized for the whole period. The long-term "water balance" value of ε was used (0.87), and no additional soil moisture impacts on *ET* were accounted for. Figure 4 compares the resulting power spectra for the simulated and observed discharge. For over 3 orders of magnitude in frequency, the power spectra are nearly identical. The power spectra of the observed and simulated streamflow both decrease with frequency and show similar peaks at 1 d^{-1} and 1 y^{-1}, reflecting the impact of diurnal and seasonal cycles in forcing, respectively. Only above frequencies of 1 d^{-1} do the power spectra start to deviate considerably. This might be due to the somewhat dampened response in simulated discharge under low-storage conditions (Figure 3).

7. Discharge Sensitivity Through Optimization

[37] The discharge sensitivity $g(Q)$ can also be obtained by optimizing the parameters in the $g(Q)$ function such that an optimal fit is obtained with the observed discharge. This can be done over the whole record using the piecewise-linear approximation of $g(Q)$, or the quadratic function proposed in the work of *Kirchner* [2009]. However by optimizing over the whole period at once, dynamic effects in the evaporation efficiency ε would need to be parameterized. Also, uncertainties in the modeling of snow processes would impact $g(Q)$. Furthermore the piecewise-linear function has many degrees of freedom, while the quadratic function of *Kirchner* [2009] can potentially lead to unusual behavior (i.e., $g(Q)$ could decrease with Q in its upper ranges). The optimization was therefore performed on monthly basis using unconstrained nonlinear optimization on a simple power law approximation of $g(Q)$, i.e., $g(Q) = \alpha Q\beta$. While a power law approximation of $g(Q)$ is not appropriate over the whole range of Q (Figure 2), it provides a useful (and low dimensional) alternative to other forms of $g(Q)$, such as the second-order polynomial used in the work of *Kirchner* [2009], for application at monthly time scales where the dynamic range of Q is limited. In addition to α and β, the evaporation efficiency ε was optimized simultaneously to avoid possible compensation for soil moisture stress and phenology in the optimized parameters.

[38] Figure 5 shows a composite estimate of $g(Q)$ based on the optimized power law relationships for individual months. Only months with a relatively low variation in discharge and with a good fit to observed discharge have been plotted in order to exclude months where snowmelt has a potential impact on $g(Q)$. On a monthly time scale, the wet (and short-lived) extremes are lacking due to the fast response times of the system at high Q. However, the same concave tendency is apparent, and in the region where $\beta \approx 1$ (Figure 2), the points align with the curve derived from the observations. The alignment of individual months in the optimized discharge sensitivity confirms the strong dependency of the system response on the system state (i.e., storage). It should be noted that the scatter in Figure 5 is not necessarily indicative of a deficiency in model structure, but can also be caused by uncertainty in observations.

8. Controls on Streamflow Changes

[39] It is of interest to study what processes are responsible for changes in streamflow. The simple dynamical systems approach used here allows for a comprehensive quantification of different controls on streamflow dynamics. Using a similar approach, *Teuling and Troch* [2005]; *Teuling et al.* [2007] quantified controls on the temporal changes in the spatial variability of soil moisture using a 1-D model of the unsaturated zone. *van Heerwaarden et al.* [2010] investigated controls on the temporal evolution of evapotranspiration using a slab model of boundary layer

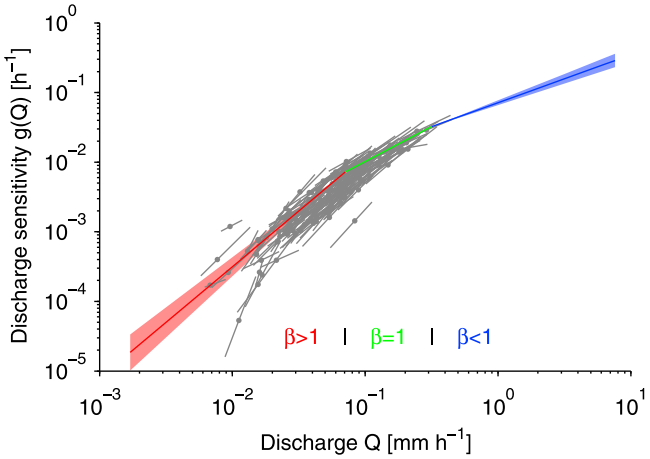

Figure 5. Optimized discharge sensitivity $g(Q)$ for Rietholzbach. Discharge sensitivity was derived from optimization of $g(Q) = \alpha Q\beta$ to observed hourly discharge for all months in the period 1976–2007. Only months are shown in which the model was able to simulate runoff below a threshold RMSE (0.3 measured in log space) and for which the difference between the 25th and 75th percentile in observed discharge was below a threshold. See text for details.

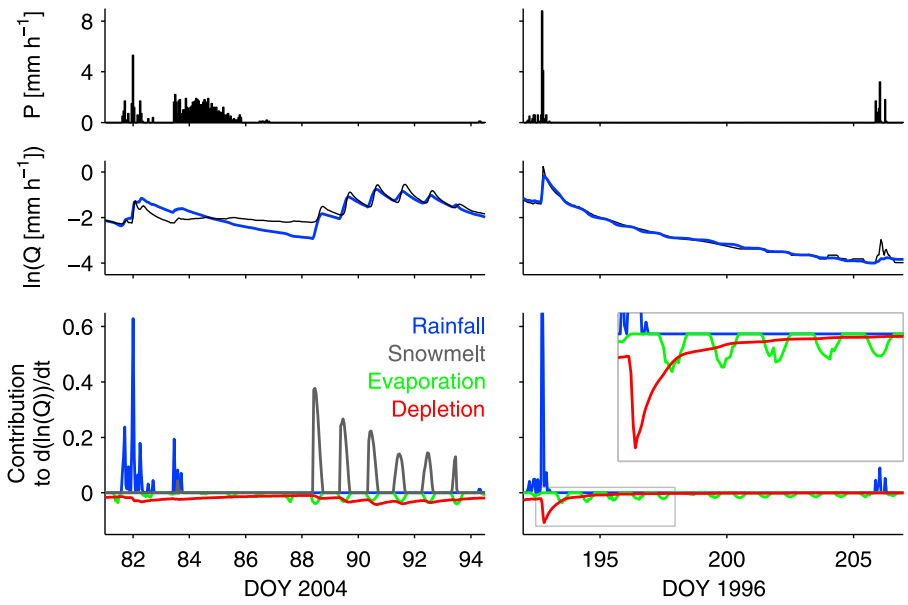

Figure 6. Attribution of changes in streamflow to different components in the water balance model following equation (19). See text for details.

growth. The streamflow rate of change equation (3) can be rewritten as:

$$\frac{dQ}{dt} = \underbrace{\alpha Q^{\beta} P}_{\text{Precipitation}} \underbrace{+\alpha Q^{\beta} M}_{\text{Snowmelt}} \underbrace{-\alpha Q^{\beta} ET}_{\text{Evaporation}} \underbrace{-\alpha Q^{\beta+1}}_{\text{Discharge}}. \quad (18)$$

[40] Alternatively, the rate of change in ln(Q) helps to reveal the contribution of "slow" processes such as evapotranspiration that have a much lower magnitude than rainfall at peak intensity. It can be written as:

$$\frac{d(\ln(Q))}{dt} = \underbrace{\alpha Q^{\beta-1} P}_{\text{Precipitation}} \underbrace{+\alpha Q^{\beta-1} M}_{\text{Snowmelt}} \underbrace{-\alpha Q^{\beta-1} ET}_{\text{Evaporation}} \underbrace{-\alpha Q^{\beta}}_{\text{Discharge}}. \quad (19)$$

[41] We investigate the controls on streamflow changes for two events with contrasting conditions. The first case includes a large snow event in late spring, while the second is a long recession after a large rainfall during summer. The simulations were performed using the optimized parameters for the corresponding month (section 7) and optimized snow parameters. The observed discharge at the beginning of each event is taken as initial condition. Figure 6 shows that changes in streamflow are typically the net result of several controls, some of which work in opposite directions. The controls all have their own typical dynamical behavior. Note that rainfall typically only acts to increase streamflow. As soon as the rain ceases, recession in streamflow is driven mainly by changes in storage induced by discharge.

[42] In absolute terms, the contribution of the evaporation term in equation (19) to changes in streamflow is small. Evapotranspiration is only the dominant term during low flow conditions, when there is no rainfall and the discharge term has become negligible. Because of the weighting with $g(Q)$, it is on average much smaller than contributions of rainfall and discharge, which generally coincide with high Q and $g(Q)$. However, when considered in time, the contribution of evapotranspiration cannot be neglected. Over the whole 32 year period, the evapotranspiration is the main driver of changes in streamflow during 21% of the time. The discharge term is dominant for 64% of the time since it is largest both after rainfall, during nighttime, and during wet conditions with low incoming radiation. Rainfall and snowmelt are only dominant during 13% and 3% of the time, respectively.

9. Inferring Catchment Storage

[43] In the conceptualization of a catchment as a simple dynamical system, storage and discharge are always uniquely related. Theoretically, this opens up the possibility of estimating storage change directly from streamflow. This could be a valuable addition to current storage change estimation methods, which mostly apply to much larger regions [*Seneviratne et al.*, 2004; *Andersen et al.*, 2005; *Hirschi et al.*, 2006; *Troch et al.*, 2007; *Mueller et al.*, 2010] or very local measurements (such as soil moisture profiles at an individual point). The tight relation between system states and outflow has also been utilized to perform data assimilation with streamflow observations [e.g., *Clark et al.*, 2008].

[44] In order to derive a functional relation between the two, recall that $g(Q) = dQ/dS$. The relation between S and Q can thus be obtained from [*Kirchner*, 2009]:

$$\int dS = \int \frac{dQ}{g(Q)}. \quad (20)$$

[45] For any range in which $g(Q)$ can be approximated by a power law (i.e., $g(Q) = \alpha\ Q\beta$), the inferred relation

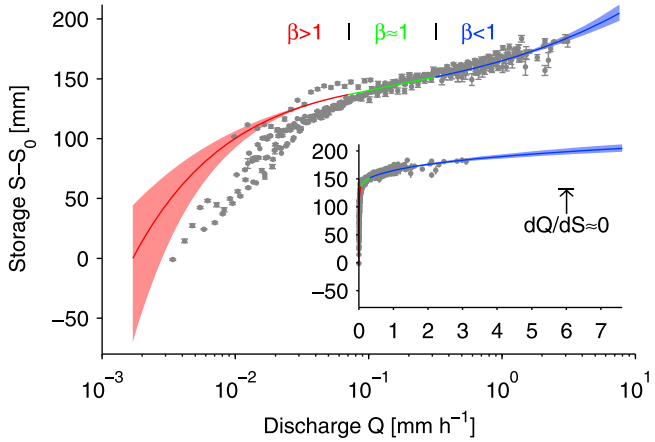

Figure 7. Relation between discharge Q and catchment storage $S - S_0$ for Rietholzbach plotted using a logaritmic and linear (inset) axis for Q. Gray points show the lysimeter storage (bin average and standard error). For each year of lysimeter data, the offset to the linear part of the curve was removed to account for possible instrument drift. Line shows the relation given by equation (22), and shading indicates the propagated uncertainty bounds of $g(Q)$ in Figure 2. Colors correspond to the different regimes for β (as in Figure 2). Note that on a linear scale, dQ/dS appears to be effectively zero over a large range of S.

between S and Q can be easily obtained through integration of equation (20):

$$S(Q) = \begin{cases} \frac{1}{\alpha}\frac{1}{1-\beta}Q^{1-\beta} + S_0, & \beta \neq 1 \\ \frac{1}{\alpha}\ln(Q) + S_0 & \beta = 1, \end{cases} \quad (21)$$

where S_0 is an arbitrary reference storage level. It should be noted that in reality the reference storage level is also arbitrary due to the absence of a lower system boundary, and storage is either considered with an arbitrary offset or in terms of its changes. For $\beta = 1$, equation (21) results in a linear relation between $\ln(Q)$ and S. This behavior is very different from that of a linear reservoir, where Q, rather than $\ln(Q)$, would be a linear function of S.

[46] From the curves in Figure 2 and by using equation (21), we find the following relation between S and Q for Rietholzbach:

$$S(Q) = \begin{cases} -3.346Q^{-0.6} + 153.18 & Q < 0.071 \\ 9.809\ln(Q) + 162.81 & 0.071 \leq Q < 0.317 \\ 45.01Q^{0.31} + 120.07 & Q \geq 0.317, \end{cases} \quad (22)$$

where the arbitrary offset is chosen such that $S = 0$ for the minimum observed Q (0.0017 mm h^{-1}, 10 September 1991), and S and Q are in mm and mm h^{-1}, respectively. Figure 7 displays the inferred storage from equation (22) along with the propagated uncertainty bounds from Figure 2. Note that since we infer storage from streamflow, S is plotted as a function of Q rather than the other way around. While the relation between $\ln(Q)$ and S is only slightly nonlinear, the uncertainty in S rapidly increases for low Q, and highlights the uncertainty of the estimation in the low soil moisture range. The inset in Figure 7 shows the relation between catchment storage and streamflow in the linear space. Its strong nonlinearity is consistent with studies in other catchments, and can lead to apparent threshold behavior in streamflow response to rainfall [*Western and Grayson*, 1998; *Tromp-van Meerveld and McDonnell*, 2006; *Seyfried et al.*, 2008; *Kirchner*, 2009].

[47] The presence of a weighing lysimeter in the catchment provides a unique opportunity to assess our inferred storage estimates. Figure 7 also compares the inferred relation between catchment storage and streamflow (equation (22)) with the relation between storage in the lysimeter and the streamflow. It should be noted that this validation is not strict, due to the discrepancy in scales: the area of the catchment is roughly a million times larger than that of the lysimeter (3.31 km^2 vs. 3.14 m^2).The lysimeter storage was corrected for yearly changes in mean storage due to possible instrument drift or grass cover. For high discharge (>10^{-1}mm h^{-1}), changes in inferred catchment storage are very similar to changes in lysimeter storage. For low discharge, the inferred storage overestimates the lysimeter storage. A possible explanation for the difference between inferred and lysimeter storage is the lack of interaction of the lysimeter with the groundwater. In addition, the lysimeter is covered by grass, while the catchment is partly covered by forest. This may induce discrepancy between estimates of evapotranspiration and storage [*Lehner et al.*, 2010].

[48] To further explore the validity of the storage estimates, we compare the dynamics of the inferred hourly storage with storage from the lysimeter, from an independent soil moisture profile, and from simulations with a uncalibrated land surface model. These simulations are added to provide a benchmark for the other estimates. The land surface model is the Variable Infiltration Capacity model (VIC, for details see *Liang et al.* [1994]), which was run with default parameters for the predominant soil type in Rietholzbach. Figure 8 shows the hourly storage dynamics for the different methods for two selected periods in Spring 2000 and 2002. The inferred storage follows the lysimeter closely after rainfall events, while VIC underestimates the storage response to rainfall, possibly due to an overestimation of direct (surface) runoff. The storage decrease during rainless periods seems to be less for the inferred storage than for the other methods. This is likely related to the problems of estimating $g(Q)$ from observations under dry conditions. In spite of these problems, the inferred storage has a larger dynamic range than the storage derived from the soil moisture profile. Under dry conditions the estimation of $g(Q)$ and subsequently of the inferred storage might benefit from considering evapotranspiration measurements, either from the lysimeter or from additional larger-scale observations, e.g., by scintillometery.

[49] The direct relation between S and Q allows for a straightforward analysis of storage dynamics at longer time scales. For the hourly storage estimates, we find a yearly average dynamic storage range of 104 mm. This is similar to values reported by *Kirchner* [2009] for the Plynlimon catchments. The maximum inferred storage range over the whole 32 year period is almost twice as large: 205 mm. Figure 9 shows the monthly storage climatology derived from streamflow. There is only little difference between the average storage in the wettest (March) and the driest (August) month. This difference is only approximately 20 mm. The distribution of monthly storage anomalies is

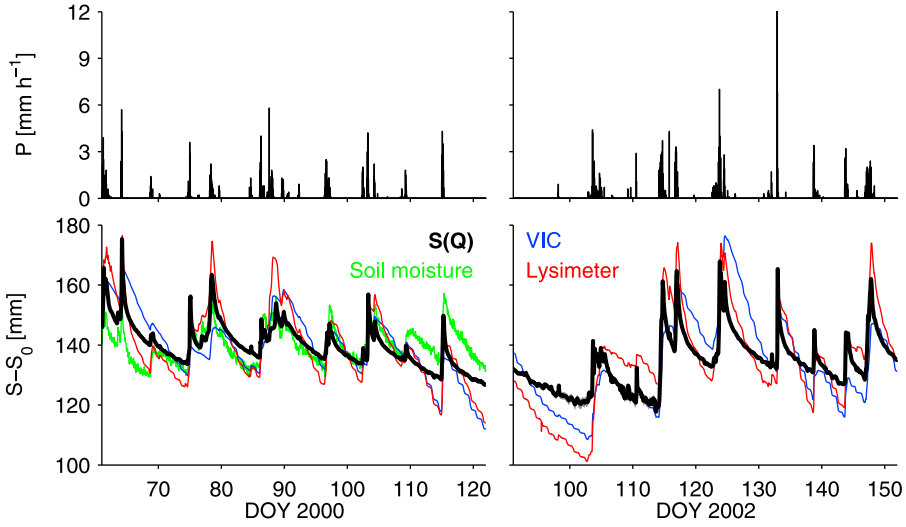

Figure 8. Storage dynamics at Rietholzbach in response to precipitation for two selected periods. (top) Observed precipitation. (bottom) Hourly storage estimates inferred from discharge by equation (22) (thick black line) with propagated uncertainty bounds (gray, small in this range of S), from a soil moisture profile (green), from the lysimeter (red), and from simulations with the variable infiltration capacity land surface model (VIC, blue).

strongly skewed, with the maximum positive anomalies being much smaller than the maximum negative anomalies. Large negative storage anomalies in general only occur in late summer. Two of the driest extremes, August 2003 and September 1991, had anomalies of −48 mm and −57 mm, respectively. As a comparison, *Andersen et al.* [2005] reported monthly storage anomalies for the 2003 heat wave derived from GRACE and averaged over Central Europe of up to −78 mm.

10. Storage Estimation and Weir Design

[50] Though it can be inferred that the derivation of discharge-based relationships become intrinsically more uncertain at low discharge, the large uncertainty in inferred storage under dry conditions is also partly an instrumentation problem. Estimation of $g(Q)$ requires estimation of changes in Q. For small Q, the sensitivity of discharge to changes in storage is very small, so that the change in storage implied by a given change in discharge is very large. This has the effect of amplifying any uncertainty in the measurement of discharge. At Rietholzbach, the uncertainty in the measurement of discharge is significant for low flow due to the unfavorable shape of the weir and due to the limited resolution of the recorded stage (cm). Since changes in storage (height of the equivalent water layer) are derived from discharge which is measured as a water height, it is relevant to focus on the relation between the two.

[51] Figure 10 shows the relation between stream stage at the weir and catchment storage derived from $S(Q)$ and the stage-discharge relationship at Rietholzbach as used by the Federal Office for the Environment. If discharge observations would be made with the sole purpose of inferring storage, a linear relationship would be desirable because of the linear error propagation. At Rietholzbach however, the relation is almost linear for high discharge (>10^{-1} mm h^{-1}), but storage becomes increasingly sensitive to stage for low discharge. The probability density function of discharge (inset Figure 10) shows that discharge in this sensitive range occurs actually most frequently (59% of the time). This makes the current infrastructure at Rietholzbach not well suited for measuring changes in storage under low-flow conditions. To increase the accuracy of measured changes in discharge under low-discharge conditions, it is possible to install two weirs in series, one of which is specially designed for high accuracy during low-flow conditions but is overflowed during high-flow conditions.

11. Inferring Precipitation and Snowmelt Rates

[52] In our simple system, discharge is a direct and invertible function of storage. This implies that changes in discharge directly reflect changes in storage (i.e., due to

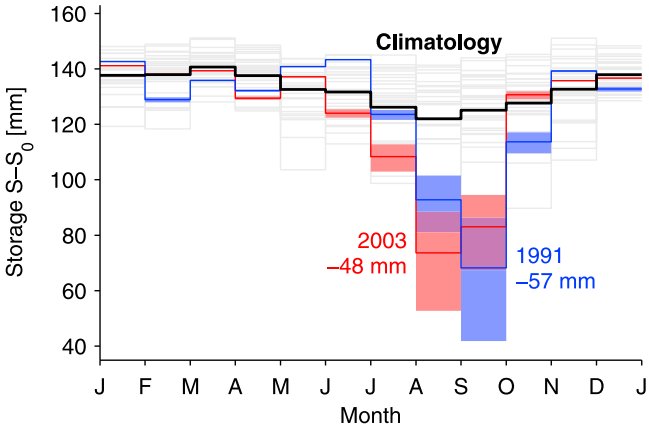

Figure 9. Inferred monthly storage climatology for Rietholzbach. The thick black line indicates the mean seasonal cycle, thin gray lines indicate the individual years, and colors indicate the extreme dry years 1991 (blue) and 2003 (red) with the shading indicating the propagated uncertainty bounds from $g(Q)$ (Figure 2).

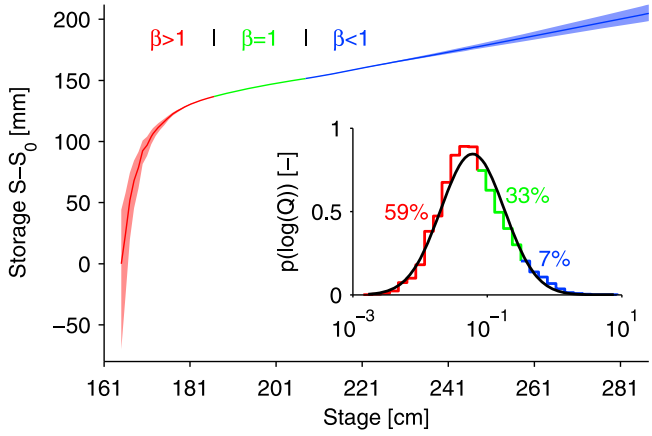

Figure 10. Relation between stage and subsurface catchment storage. Note that storage becomes very sensitive to changes in stage because the sensitivity of discharge to storage is low when the catchment is dry. The inset shows the probability density distribution of hourly discharge. The tick line indicates a fitted (log)normal distribution.

infiltration). Since our system is simple enough to be invertible, it is possible to infer fluxes of water at the land surface directly from subsequent observations of streamflow, following the approach outlined in the work of *Kirchner* [2009]. Rearranging equation (3) yields:

$$P + M - ET = \frac{\mathrm{d}Q/\mathrm{d}t}{g(Q)} + Q. \tag{23}$$

When applying equation (23), all terms on the right-hand side have to be estimated from streamflow at discrete points in time. When neglecting the possible time lag between changes in catchment storage and changes in streamflow at the weir, the net flux at the land surface can be estimated through:

$$P_t + M_t - ET_t \approx \frac{(Q_{t+1} - Q_{t-1})/2}{[g(Q_{t+1}) + g(Q_{t-1})]/2} + (Q_{t+1} + Q_{t-1})/2. \tag{24}$$

[53] The magnitude of the individual fluxes P, M, and ET can be estimated at times when two of the fluxes can be neglected. For instance during the warm season ($M \approx 0$), P can be estimated during times when $P - ET$ exceeds zero ($P - ET \approx P$):

$$P_t \approx \max\left(0, \frac{(Q_{t+1} - Q_{t-1})/2}{[g(Q_{t+1}) + g(Q_{t-1})]/2} + (Q_{t+1} + Q_{t-1})/2\right). \tag{25}$$

[54] In special conditions, namely when snowmelt occurs relatively fast and without any additional input from precipitation, snowmelt intensity M can be inferred from streamflow fluctuations in a similar way as precipitation:

$$M_t \approx \max\left(0, \frac{(Q_{t+1} - Q_{t-1})/2}{[g(Q_{t+1}) + g(Q_{t-1})]/2} + (Q_{t+1} + Q_{t-1})/2\right). \tag{26}$$

[55] Theoretically, ET can be estimated in a similar way. However, typical intensities of ET (order 10^{-1} mm h^{-1}) are generally much smaller than that of P and M (>10^{0} mm h^{-1}, see also Figure 12), making the inference of ET more sensitive to deficiencies in our simple systems representation of real catchment processes and measurement resolution (see section 12).

[56] Figure 11 shows the observed and inferred (equation (25)) precipitation rates for four selected cases. Among these four cases are the largest recorded hourly precipitation sum (37.2 mm, 6 July 1994), and the highest daily sum (11 May 1999). In all cases, equation (25) predicts the correct timing and magnitude of the rainfall over at least an order of magnitude. Since no time lag is taken into account, the inferred precipitation can respond slightly earlier than the observed since P_t in equation (25) is calculated partly based on Q_{t+1}. However, by introducing a 1 h lag, the inferred precipitation lags behind the observations by a larger margin (not shown). This suggests the time lag to be small for Rietholzbach. Inferred precipitation amounts seem to slightly underestimate the observed precipitation. This can be caused by small errors in $g(Q)$, but also because part of the precipitation is intercepted and does not contribute to the subsurface storage that controls streamflow.

[57] Figure 12 shows three examples for Rietholzbach in which snowmelt has a strong and unambiguous effect on streamflow, and in which hourly snowmelt can be inferred from streamflow fluctuations. First of all, the presence of snow significantly impacts the streamflow dynamics. When all precipitation would be liquid, the streamflow would follow precipitation inputs (light green lines). In the simulations with snow, as well as in the observations, streamflow decreases first, only to increase after a number of days under a strong diurnal cycle. The results from the snowmelt simulations confirm that this strong diurnal cycle can be fully explained by snowmelt. The inferred snowmelt is also consistent in terms of timing, magnitude and duration with the simulated snowmelt. It should be noted that the inferred snowmelt sums over the melt period closely match the recorded precipitation (which includes snow).

12. Diurnal Streamflow Fluctuations

[58] In our simple dynamical systems approach evapotranspiration losses impact storage and thus streamflow.

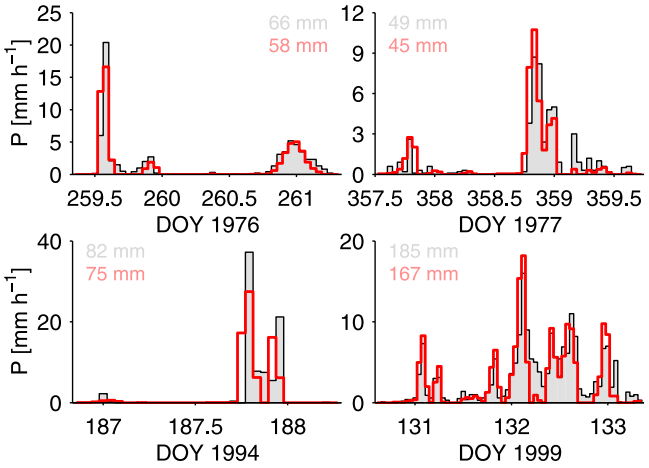

Figure 11. Observed (black line) and inferred (thick red line) precipitation from streamflow using equation (25) for four selected cases (see text for details).

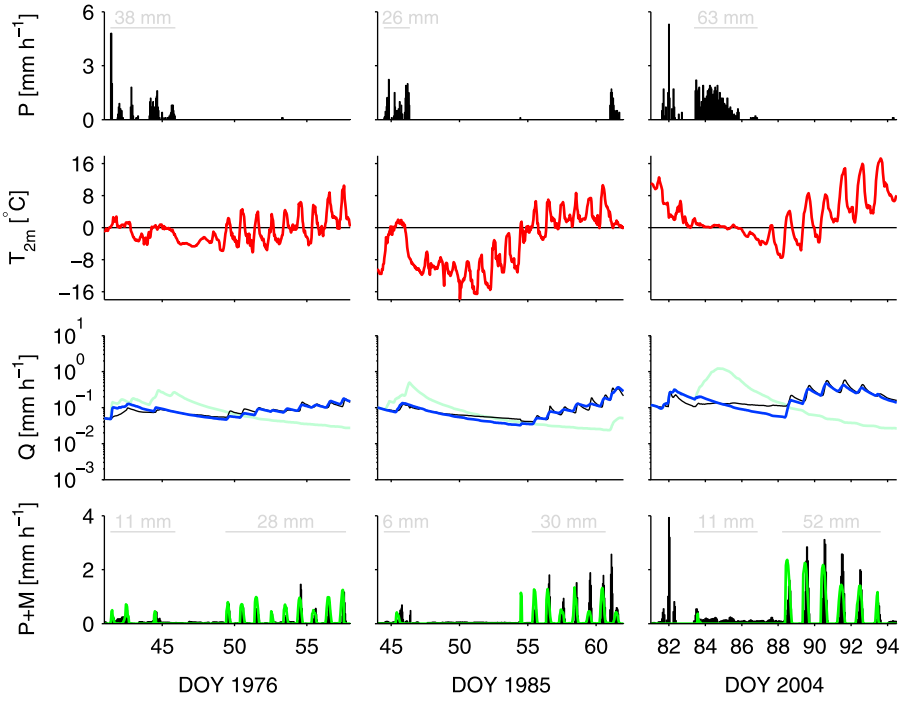

Figure 12. Impact of snow on streamflow and inferred rates of snowmelt from streamflow using equation (26) for three selected cases in (left) 1976, (middle) 1985, and (right) 2004. Observed precipitation P (including snowfall). Observed 2 m temperature T_{2m}. Observed discharge Q (thin black line) and simulated discharge with optimized melt parameters (thick blue line) and without any snow processes (light green line). Inferred precipitation and snowmelt $P + M$ (black lines) and melt from simulations (green). Sums for P and $P + M$ are indicated in light gray for selected periods.

Since evapotranspiration follows a marked diurnal cycle, the streamflow can also be expected to reflect this cycle. Figure 13 shows two examples for the year 1991 of how the diurnal cycle of evapotranspiration impacts streamflow.

[59] Figure 13 (left) illustrates a situation with high subsurface storage and as a result high discharge. More specifically, the discharge is much larger than the evapotranspiration even at the time of day where ET is maximum. In this situation, discharge is the dominant system loss and the signature of other losses (i.e., ET) on streamflow is small. It is likely that streamflow recession is somewhat influenced by ET, but this effect is too small to be detected by eye.

[60] In contrast, Figure 13 (middle) shows data for a period in the same year when streamflow is 2 orders of magnitude smaller than in Figure 13 (left). Here, ET is more than a magnitude larger than Q for a large part of the day. There is a strong diurnal cycle apparent in the streamflow time series in response to the ET losses from the system. Specifically, $dQ/dt > 0$ during recession, which conflicts with the simple dynamical systems approach (in which storage and thus discharge should be continuously decreasing in the absence of precipitation or snowmelt inputs). When the diurnal cycle is removed from the observations by taking a 24 h moving average, the dynamics are again in correspondence with those of the simple dynamical system.

[61] Our explanation for this phenomenon is the one proposed by *Kirchner* [2009]: that discharge is influenced most directly by storage in the near-stream riparian zone, which is continually recharged by drainage from upslope, with evapotranspiration losses leading to net declines in storage (and thus streamflow) during the day, and net recharge from upslope leading to net increases in storage (and thus streamflow) at night, when evapotranspiration rates are much lower.

[62] Figure 13 (right) shows a composite of streamflow on rainless summer days (JJA, 1976–2007) as function of time of day. Here all recessions have been averaged into equally spaced bins in logspace. Three bin averages are highlighted: one at high Q where no clear diurnal cycle is visible, one at intermediate flow where a diurnal cycle is apparent but $dQ/dt \leq 0$ at all times, and one at low flow where a strong diurnal cycle is visible and $dQ/dt > 0$ during nighttime. Note that the time of maximum streamflow shifts from late night to noon with decreasing average streamflow.

13. Extreme Discharge Events

[63] Although the key assumption of our approach, namely that discharge is directly and uniquely related to the total catchment storage, might be appropriate in the Rietholzbach under most conditions, it might be less appropriate under conditions where runoff generating mechanisms come into play that are not directly related to water in the subsurface. One example is a rain storm of an intensity and duration such that infiltration excess runoff occurs. Such events are often associated with extreme peak discharges. Therefore we investigate whether our approach can successfully capture the dynamics of discharge as well as the magnitude of its peaks. Note that these peaks occur in the range where $g(Q)$ has been extrapolated. We consider two cases: one which contains the highest observed discharge and one which contains the highest simulated dis-

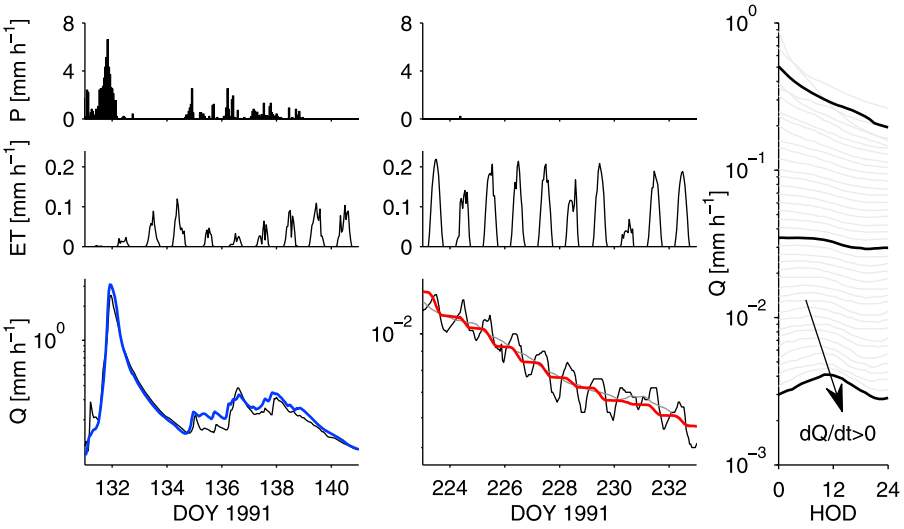

Figure 13. Streamflow recession and diurnal fluctuations. Two examples for 1991 show streamflow during (left) wet and (middle) dry conditions. (top) Precipitation P, (middle) lysimeter evapotranspiration ET, and (bottom) observed (thin black line) and simulated (thick blue and red lines) discharge Q on a log axis. The parameters result from monthly optimization: (left) $\alpha = -0.95$, $\beta = 1.14$, and $\varepsilon = 0.33$ (May 1991) and (middle) $\alpha = 0.58$, $\beta = 1.88$, and $\varepsilon = 0.42$ (August 1991). (right) A composite of daily streamflow recessions as a function of hour of day (HOD, see text for details). Note the daily fluctuations with $dQ/dt > 0$ only occur at low Q. The thin gray line in Figure 13 (bottom middle) shows the 24 h moving average observed streamflow.

charge in the 32 year continuous simulation, with $g(Q)$ as given by equation (9).

[64] The case with the highest simulated discharge is shown in Figure 14 (left). In this case, the simulated discharge largely follows the observed discharge, and the magnitude of the discharge peaks is almost identical. This shows that the method is able to simulate extreme peak discharge beyond the range of moderate discharges used to estimate $g(Q)$, provided that the rainfall intensity allows for most of the water to infiltrate and impact the runoff via pathways that are controlled by storage. The error made by extrapolation of $g(Q)$ to peak discharges is small as indicated by the propagated error bounds. The second case (Figure 14, right) deals with the highest observed discharge peak, which coincides with the highest observed hourly precipitation intensity (nearly 40 mm h^{-1}, see also Figure 11). Note that this event is extreme and unprecedented in the 32 year record. In this extreme case, the continuous simulations miss the timing and magnitude of the discharge peak. Simulations with increased initial storage show that this cannot be attributed to an underestimation of storage at the start of the event or to uncertainty in $g(Q)$. Note that the discharge rapidly decreases after the initial peak while the precipitation level remains at 5 mm h^{-1}. In our model, discharge should always increase as long as the precipitation intensity exceeds the discharge. This suggests that the initial peak was caused by processes not directly linked to catchment storage, such as infiltration excess runoff.

14. Concluding Remarks

[65] Based on 32 years of discharge observations, the hydrological response of the Swiss Rietholzbach catchment can to the first order be characterized as that of a simple dynamical system following *Kirchner* [2009]. In this system, discharge is predominantly a function of subsurface storage in the catchment. This function is strongly nonlinear. At low-catchment storage, streamflow shows little response to precipitation. Under high-storage conditions, the streamflow responds much stronger to a similar precipitation event. The discharge sensitivity is also concave-downward in the log space. At low discharge, the logarithm of the discharge sensitivity changes rapidly, while at high discharge the log of the sensitivity is a shallower function of discharge.

[66] The direct relationship between storage and discharge allows catchment storage to be estimated from

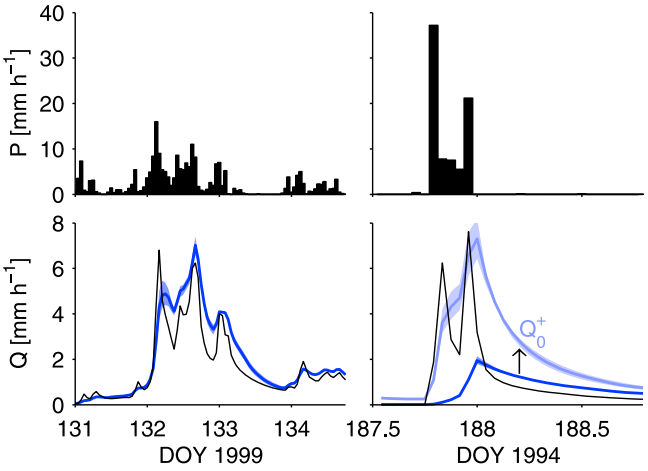

Figure 14. Extreme discharge events at Rietholzbach. (top) Precipitation. (bottom) Observed (thin black line) and simulated (thick blue line) discharge Q. Shaded area indicate the propagated uncertainty bounds of $g(Q)$ in Figure 2. (bottom right) The lighter blue curve and shading indicate simulations with higher initial discharge (Q_0^+).

streamflow. While storage at the catchment scale cannot be directly validated, the inferred storage shows good agreement with storage as recorded by a weighing lysimeter in the catchment, and with simulations of a land surface model. The method can also be used to estimate rates of precipitation and snowmelt. Inferred precipitation rates correspond in timing and amount to rain gauge observations. This opens the possibility to use streamflow variations to monitor precipitation at the small catchment scale. Inferred rates of snowmelt for three selected cases also show good correspondence to simulated snowmelt in terms of inferred amount, timing, and diurnal cycle.

[67] While the Rietholzbach catchment behaves almost perfectly like a simple dynamical system under wet conditions, it does less so under dry conditions. Runoff peaks after rainfall, when plotted on log axes, are often stronger than would be expected based on the discharge sensitivity alone. This can be explained by the increased importance of "rapid" pathways such as overland flow and interflow, all of which lead to direct runoff without any dependence on the catchment subsurface storage. Also, the simple dynamical systems approach does not give an explanation for the observed diurnal fluctuations in streamflow under dry conditions. These fluctuations are likely caused by the interplay between the saturated areas directly surrounding the stream (which respond rapidly to evapotranspiration), and the rest of the catchment where the response to evapotranspiration is dampened. It should be noted that both deficiencies only are apparent when discharge is evaluated in the log space. In the linear space, these contributions are still negligible and the model performs well even under dry conditions.

[68] The low accuracy of the discharge observations adds to the intrinsic decrease in accuracy of the applied method at low flows. Future studies on catchment-scale storage dynamics in the Rietholzbach and other similar catchments would benefit from an increased accuracy of low-flow discharge observations. Such increased accuracy can for instance be achieved by installing a second weir, especially designed for low flows, "in series" with the existing weir.

[69] While our approach can reproduce streamflow and storage dynamics over a range of temporal scales, it is not superior to other modeling concepts. For instance, the approach cannot explain the complexity in travel times of water observed in various catchments. Other, more complex, modeling approaches might therefore be more appropriate depending on the question to be addressed.

[70] **Acknowledgments.** Ruud Hurkmans is acknowledged for providing simulations with VIC. A.J.T. acknowledges partial financial support from the Netherlands Organization for Scientific Research (NWO) through a Rubicon grant. We thank Remko Uijlenhoet and Claudia Brauer and several anonymous reviewers for their comments.

References

Andersen, O. B., S. I. Seneviratne, J. Hinderer, and P. Viterbo (2005), GRACE-derived terrestrial water storage depletion associated with the 2003 European heat wave, *Geophys. Res. Lett.*, *32*, L18405, doi:10.1029/2005GL023574.

Beldring, S., L. Gottschalk, J. Seibert, and L. M. Tallaksen (1999), Distribution of soil moisture and groundwater levels at patch and catchment scales, *Agric. For. Meteorol.*, *98–99*, 305–324.

Bogaart, P. W., A. J. Teuling, and P. A. Troch (2008), A state-dependent parameterization of saturated-unsaturated zone interaction, *Water Resour. Res.*, *44*, W11423, doi:10.1029/2007WR006487.

Brutsaert, W., and J. L. Nieber (1977), Regionalized drought flow hydrographs from a mature glaciated plateau, *Water Resour. Res.*, *13*(3), 637–643.

Calanca, P. (2004), Interannual variability of summer mean soil moisture conditions in Switzerland during the 20th century: A look using a stochastic soil moisture model, *Water Resour. Res.*, *40*, W12502, doi:10.1029/2004WR003254.

Clark, M. P., D. E. Rupp, R. A. Woods, X. Zheng, R. P. Ibbitt, A. G. Slater, J. Schmidt, and M. J. Uddstrom (2008), Hydrological data assimilation with the ensemble Kalman filter: Use of streamflow observations to update states in a distributed hydrological model, *Adv. Water Resour.*, *31*(10), 1309–1324, doi:10.1016/j.advwatres.2008.06.005.

Daniel, J. F. (1976), Estimating groundwater evapotranspiration from streamflow records, *Water Resour. Res.*, *12*(3), 360–364.

Federer, C. A. (1973), Forest transpiration greatly speeds streamflow recession, *Water Resour. Res.*, *9*(6), 1599–1604.

Germann, P. (1981), Untersuchungen über den Bodenwasserhaushalt im hydrologischen Einzugsgebiet Rietholzbach, Ph.D. thesis, 137 pp., ETH Zurich, Zurich, Switzerland.

Gurtz, J., M. Zappa, K. Jasper, H. Lang, M. Verbunt, A. Badoux, and T. Vitvar (2003), A comparative study in modelling runoff and its components in two mountainous catchments, *Hydrol. Process.*, *17*(2), 297–311, doi:10.1002/hyp.1125.

Hall, F. R. (1968), Base flow recessions—A review, *Water Resour. Res.*, *4*(5), 973–983.

Hirschi, M., S. I. Seneviratne, and C. Schär (2006), Seasonal variations in terrestrial water storage for major midlatitude river basins, *J. Hydrometeorol.*, *7*(1), 39–60.

Kirchner, J. W. (2006), Getting the right answers for the right reasons: Linking measurements, analyses, and models to advance the science of hydrology, *Water Resour. Res.*, *42*, W03S04, doi:10.1029/2005WR004362.

Kirchner, J. W. (2009), Catchments as simple dynamical systems: Catchment characterization, rainfall-runoff modeling, and doing hydrology backward, *Water Resour. Res.*, *45*, W02429, doi:10.1029/2008WR006912.

Kustas, W. P., A. Rango, and R. Uijlenhoet (1994), A simple energy budget algorithm for the snowmelt runoff model, *Water Resour. Res.*, *30*(5), 1515–1527.

Lehner, I., A. J. Teuling, J. Gurtz, and S. I. Seneviratne (2010), Long-term water balance in the prealpine Rietholzbach catchment: First comparison of evapotranspiration estimates, in *Status and Perspectives of Hydrology in Small Basins, 30 March–2 April 2009*, *IAHS Publ. 336*, Goslar-Hahnenklee, Germany.

Liang, X., D. P. Lettenmaier, E. F. Wood, and S. J. Burges (1994), A simple hydrologically based model of land surface water and energy fluxes for general circulation models, *J. Geophys. Res.*, *99*(D7), 14,415–14,428, doi:10.1029/94JD00483.

Lyon, S. W., G. Destouni, R. Giesler, C. Humborg, M. Mörth, J. Seibert, J. Karlsson, and P. A. Troch (2009), Estimation of permafrost thawing rates in a subarctic catchment using recession flow analysis, *Hydrol. Earth Syst. Sci.*, *13*(5), 595–604.

Mueller, B., M. Hirschi, and S. I. Seneviratne (2010), New diagnostic estimates of variations in terrestrial water storage based on ERA-Interim data, *Hydrol. Process.*, in press.

Seneviratne, S. I., P. Viterbo, D. Lüthi, and C. Schär (2004), Inferring changes in terrestrial water storage using ERA-40 reanalysis data: The Mississippi River basin, *J. Clim.*, *17*(11), 2039–2057.

Seyfried, M. S., L. E. Grant, D. Marks, A. Winstral, and J. McNamara (2008), Simulated soil water storage effects on streamflow generation in a mountainous snowmelt environment, Idaho, USA, *Hydrol. Process.*, *23*(6), 858–873, doi:10.1002/hyp.7211.

Sivapalan, M., G. Blöschl, L. Zhang, and R. Vertessy (2003), Downward approach to hydrological prediction, *Hydrol. Process.*, *17*(11), 2101–2111, doi:10.1002/hyp.1425.

Tallaksen, L. M. (1995), A review of baseflow recession analysis, *J. Hydrol.*, *165*(1–4), 349–370.

Teuling, A. J., and P. A. Troch (2005), Improved understanding of soil moisture variability dynamics, *Geophys. Res. Lett.*, *32*, L05404, doi:10.1029/2004GL021935.

Teuling, A. J., S. I. Seneviratne, C. Williams, and P. A. Troch (2006), Observed timescales of evapotranspiration response to soil moisture, *Geophys. Res. Lett.*, *33*, L23403, doi:10.1029/2006GL028178.

Teuling, A. J., F. Hupet, R. Uijlenhoet, and P. A. Troch (2007), Climate variability effects on spatial soil moisture dynamics, *Geophys. Res. Lett.*, *34*, L06406, doi:10.1029/2006GL029080.

Teuling, A. J., et al. (2009), A regional perspective on trends in continental evaporation, *Geophys. Res. Lett.*, *36*, L02404, doi:10.1029/2008GL036584.

Troch, P. A., M. Durcik, S. I. Seneviratne, M. Hirschi, A. J. Teuling, R. Hurkmans, and S. Hasan (2007), New data sets to improve terrestrial water storage change estimation, *Eos Trans. AGU*, *88*(45), 469–470, doi:10.1029/2007EO450001.

Tromp-van Meerveld, H. J., and J. J. McDonnell (2006), Threshold relations in subsurface stormflow: 2. The fill and spill hypothesis, *Water Resour. Res.*, *42*, W02411, doi:10.1029/2004WR003800.

van Heerwaarden, C. C., J. Vilà-Guerau de Arellano, A. Gounou, F. Guichard, and F. Couvreux (2010), Understanding the daily cycle of evapotranspiration: A method to quantify the influence of forcings and feedbacks, *J. Hydrometeorol.*, doi:10.1175/2010JHM1272.1, in press.

Western, A. W., and R. B. Grayson (1998), The Tarrawarra data set: Soil moisture patterns, soil characteristics, and hydrological flux measurements, *Water. Resour. Res.*, *34*(10), 2765–2768.

Wittenberg, H., and M. Sivapalan (1999), Watershed groundwater balance estimation using streamflow recession analysis and baseflow separation, *J. Hydrol.*, *219*(1–2), 20–33.

J. W. Kirchner, Swiss Federal Institute for Forest, Snow, and Landscape Research WSL, CH-8903 Birmensdorf, Switzerland.

I. Lehner, S. I. Seneviratne, and A. J. Teuling, Institute for Atmospheric and Climate Science, ETH Zurich, CHN N 16.2, Universitätstrasse 16, CH-8092 Zürich, Switzerland. (sonia.seneviratne@env.ethz.ch; ryan.teuling@env.ethz.ch)